Self-diffusion of Brownian particles in concentrated suspensions under shear

G. Bossis
Laboratoire de Physique de la Matière Condensée, Université de Nice, Parc Valrose, 06034 Nice Cedex, France

J. F. Brady
Department of Chemical Engineering, California Institute of Technology, Pasadena, California 91125

(Received 15 May 1987; accepted 29 July 1987)

The self-diffusivity of Brownian hard spheres in a simple shear flow is studied by numerical simulation. Particle trajectories are calculated by Stokesian dynamics, with an accurate representation of the suspension hydrodynamics that includes both many-body interactions and lubrication. The simulations are of a monolayer of identical spheres as a function of the Péclet number: $\mathrm{Pe} = \dot{\gamma}a^2/D_0$, which measures the relative importance of shear and Brownian forces. Here $\dot{\gamma}$ is the shear rate, a the particle radius, and D_0 the diffusion coefficient of a single sphere at infinite dilution. In the absence of shear, using only hydrodynamic interactions, the simulations reproduce the pair-distribution function of the equivalent hard-disk system. Both short- and long-time self-diffusivities are determined as a function of the Péclet number. The results show a clear transition from a Brownian motion dominated regime ($\mathrm{Pe} < 1$) to a hydrodynamically dominated regime ($\mathrm{Pe} > 10$) with a dramatic change in the behavior of the long-time self-diffusivity.

I. INTRODUCTION

Colloidal dispersions—micron-sized particles suspended in a fluid medium—are prevalent in a variety of natural and man-made settings. One of the central issues in colloid science is to understand and predict the macroscopic behavior of such systems from a knowledge of the fundamental microstructural mechanics—i.e., from the interactions among the particles and from their distribution in space and time. Considerable progress has been (and will continue to be) made in understanding the *equilibrium* properties of dispersions, for the suspended particles may be treated as a thermodynamic system and the well-developed apparatus of statistical thermodynamics can be applied. The new and interesting features come about because of the different nature of the interparticle forces in colloidal systems, e.g., London–van der Waals, screened electrostatic, etc. Of equal interest and importance, however, are the *nonequilibrium* or transport properties of dispersions, e.g., diffusion, rheology, aggregation, etc. Here our understanding is more limited, primarily for two reasons. First, the inherent nonequilibrium nature of the problem, particularly for systems far from equilibrium as in aggregation, makes theoretical developments difficult. This feature is also present in atomic or molecular systems and has given rise to the still developing area of nonequilibrium thermodynamics. Second, in colloidal dispersions particles interact via continuum-scale hydrodynamic forces, which can be quite complex, and experience random motion due to Brownian forces. There is no direct counterpart of these latter forces in molecular systems.

The purpose of this paper is to present a general framework for studying both equilibrium and nonequilibrium properties of colloidal dispersions through numerical simulation. This is accomplished by extending our previously developed method for dynamically simulating hydrodynamically interacting particles, known as Stokesian dynamics,[1,2] to include Brownian motion. The general method can be applied to a wide variety of colloidal problems and will be illustrated here by the problem indicated in the title of the self-diffusion of Brownian particles in concentrated suspensions. Self-diffusion is one of the most basic properties of colloidal dispersions. It can convey static information, through the short-time diffusivity measuring properties of the local (equilibrium) structure, as well as dynamic information in the behavior of the long-time diffusivity, as a particle must wander far from its starting point deforming the local structure and exchanging places with its neighbors. Experimentally, measurements of self-diffusion coefficients by dynamic light scattering are used to infer particle size and/or shape and information about the interparticle forces.[3] Theoretically, predicting the self-diffusion coefficient and its dependence on concentration has been of concern to statistical mechanicians and fluid dynamicists for many years.[4]

Nonequilibrium molecular dynamics has emerged as a useful tool for studying the transport properties of simple fluids like methane, argon, etc.[5–7] These simulations aid greatly in understanding transport properties, such as viscosity and normal stresses, in terms of the interparticle forces and the deformation and relaxation of the particle distribution. While feasible in principle, extending such techniques to colloidal systems, where there are large, macroscopic particles (1 nm–10 μm in size) suspended in a solvent of smaller particles or molecules, would be extremely difficult to carry out in practice. If the interest is in the behavior of a single colloidal particle, i.e., a suspension of such particles at infinite dilution, then a direct carry over of molecular dynamics might be possible. The primary interest, however, is not in isolated particles, but rather in the statis-

 0021-9606/87/215437-12$02.10

tics of a suspension of many interacting colloidal particles. Not only would the direct simulation of such a system pose an enormous computational problem, the results would contain much more information than is desired or needed to understand the behavior of the colloidal dispersion.

An alternative approach is to model the colloidal system as a suspension of macroscopic particles dispersed in a continuum Newtonian fluid. The particles interact through both interparticle colloidal forces *and* hydrodynamic forces transmitted via the continuum fluid. The particles also receive fluctuating thermal forces from the fluid that give rise to the familiar phenomenon of Brownian motion. This is the essence behind the so-called "Brownian dynamics" simulations pioneered by Ermak and McCammon[8] and further developed and employed by Dickinson and others.[9–15]

In such an approach the deterministic equations for the motion of the colloidal particles (and solvent molecules) are replaced by an N-body Langevin equation in which the random forcing is related to the temperature of the medium through the fluctuation dissipation theorem. It is possible to integrate this equation over a time step that is large compared to the momentum relaxation time characteristic of the Brownian motion τ but is small compared to the time over which the configuration of particles changes, to obtain an evolution equation for the configuration of the N colloidal particles (cf. Sec. II). The evolution equation describes the "macroscopic" motion of the particles, the rapid motions associated with the fluctuating thermal forces having been smoothed over the long time scale.

As shown in Sec. II, the central element that enters into the dynamics of the colloidal particles is the hydrodynamic mobility tensor $\mathbf{M}$, relating the velocity of each particle to the forces exerted by *all* the particles on the fluid. Thus, the problem reduces to obtaining an expression for the many-body, configuration-dependent mobility tensor from a solution to Stokes equations. (For the colloidal systems normally encountered, the smallness of the particle size results in very small particle Reynolds numbers and the reduction of the Navier–Stokes equations to the inertialess Stokes equations.) Previous investigations[8–15] have generally either treated the particles as hydrodynamically independent, and therefore used a constant (nondimensional) mobility $\mathbf{M}=\mathbf{I}$, where $\mathbf{I}$ is the unit isotropic tensor, or used a far-field asymptotic form for the interaction between two particles, such as the Oseen or Rotne–Prager tensors. While these may be accurate for dilute systems, they lack two features necessary to properly model the hydrodynamics of concentrated suspensions: many-body interactions and lubrication.

There have been several theoretical studies, most notably those of Beenakker and Mazur, that have demonstrated the importance of three- and many-body hydrodynamic interactions on the diffusion of Brownian particles.[16–21] This importance is most clearly demonstrated by the calculation of Glendinning and Russel[21] where they show that using pairwise additive hydrodynamic interactions the collective-diffusion coefficient for hard spheres become *negative* above a volume fraction of approximately 0.27. For self-diffusion the same analysis results in a physically impossible negative self-diffusion coefficient for $\phi > 0.42$. In addition to many-body hydrodynamic interactions, lubrication forces play a predominant role in determining suspension structure and behavior at high concentrations. Lubrication forces, as the name implies, result from the thin layer of viscous fluid that separates the surfaces of nearly touching particles and results in, among other effects, the relative mobility or diffusion of particles becoming zero as the particle surfaces approach one another. Thus, to accurately model the behavior of Brownian particles in suspension, both of these important hydrodynamic effects need to be addressed. Our recently developed Stokesian dynamics method has been constructed for just such a purpose.

In Sec. II we shall present the general method for simulating colloidal particles dispersed in a fluid and discuss the many-body hydrodynamic problem. The appropriate averages defining the short-time self-diffusion coefficient $\mathbf{D}_0^s$ and the long-time self-diffusion coefficient $\mathbf{D}_\infty^s$ will also be presented. (The collective-diffusion coefficient $\mathbf{D}^c$, relating particle flux to a gradient in concentration, will not be discussed here.) In Sec. III we shall present the results of our simulation study of a monolayer of identical hard spheres subjected to a simple shear flow. We shall see that the microstructure predicted by simulation in the absence of shear flow, i.e., $\mathrm{Pe}=0$, agrees well with that of a hard-disk fluid obtained by a Monte Carlo method at the same areal fraction. Here the Péclet number $\mathrm{Pe}=\dot{\gamma}a^2/D_0$ measures the relative importance of shear and Brownian forces; $\dot{\gamma}$ is the shear rate, a the particle radius, and D_0 the diffusion coefficient of a single sphere at infinite dilution. As the Péclet number increases we shall see that there is a continuous transition from a Brownian motion dominated regime ($\mathrm{Pe}<1$) to a hydrodynamically dominated regime ($\mathrm{Pe}>10$). This is most apparent in the long-time self-diffusion results where $D^s_\infty \sim O(D_0)$ as $\mathrm{Pe}\to 0$, and $D^s_\infty \sim O(\dot{\gamma}a^2)$ as $\mathrm{Pe}\to\infty$. There is also a considerable decrease in the short-time self-diffusion coefficient with increasing Péclet number owing to the formation of closely packed aggregates that reduce particle mobility. At $\mathrm{Pe}=0$ we shall also see, as expected, that the long-time self-diffusion coefficient is considerably smaller than the short-time self-diffusion coefficient, in agreement with the recent tracer diffusion experiments of van Megen, Underwood, and Snook.[22]

II. STOKESIAN DYNAMICS WITH BROWNIAN MOTION

A. Problem formulation

We consider N rigid particles suspended in an incompressible Newtonian fluid of viscosity η and density ρ. The motion of the fluid is governed by the Navier–Stokes equations, while the particle motion is described by the coupled N-body Lengevin equation, which can be written in the following form:

$$\mathbf{m}\cdot\frac{d\mathbf{U}}{dt}=\mathbf{F}^H+\mathbf{F}^P+\mathbf{F}^B, \tag{1}$$

which simply states: mass $\times$ acceleration equals the sum of the forces. In Eq. (1) $\mathbf{m}$ is a generalized mass/moment of inertia matrix of dimension $6N\times 6N$, $\mathbf{U}$ is the particle translational/rotational velocity vector of dimension $6N$, and the

$6N$ force/torque vectors $\mathbf{F}$ represent: (1) the hydrodynamic forces $\mathbf{F}^H$ exerted on the particles due to motion of and relative to the fluid, (2) the deterministic nonhydrodynamic forces $\mathbf{F}^P$, which may be either interparticle or external, and (3) the stochastic forces $\mathbf{F}^B$ that give rise to Brownian motion.

For colloidal particles the motion on the particle scale is generally such that the particle Reynolds number is small. (See below for an exact specification of this condition.) Under this condition the hydrodynamic force exerted on the particles in a suspension undergoing a bulk linear shear flow is[1,23,24]

$$\mathbf{F}^H = -\mathbf{R}_{FU}\cdot(\mathbf{U}-\mathbf{U}^\infty) + \mathbf{R}_{FE}:\mathbf{E}^\infty . \tag{2}$$

Here, $\mathbf{U}^\infty$ is the velocity of the bulk shear flow evaluated at the particle center, i.e., $\mathbf{U}_\alpha^\infty = \Omega^\infty$ for rotation and $\mathbf{U}_\alpha^\infty = \mathbf{E}^\infty\cdot\mathbf{x}_\alpha$ for translation, where $\mathbf{x}_\alpha$ is the position vector of the αth particle. $\mathbf{E}^\infty(t)$ and $\Omega^\infty(t)$ are, respectively, the symmetric (and traceless from continuity) and antisymmetric parts of the velocity gradient tensor and are constant in space, but may be arbitrary functions of time. $\mathbf{R}_{FU}(\mathbf{x})$ and $\mathbf{R}_{FE}(\mathbf{x})$ are the configuration dependent resistance matrices that give the hydrodynamic force/torque on the particles due to their motion relative to the fluid ($\mathbf{R}_{FU}$) and due to the imposed shear flow ($\mathbf{R}_{FE}$). $\mathbf{x}$ represents the generalized configuration vector specifying the location *and* orientation of all N particles. The inverse of the resistance matrix $\mathbf{R}_{FU}$ is known as the mobility matrix $\mathbf{M}(=\mathbf{R}_{FU}^{-1})$ and is a central element describing the hydrodynamic interactions among particles. Note, the subscripts on the matrices indicate the coupling between kinematic ($\mathbf{U}$) and dynamic ($\mathbf{F}$) quantities.

The deterministic nonhydrodynamic force $\mathbf{F}^P$ is arbitrary and may be most any form of interparticle or external force. The stochastic or Brownian force $\mathbf{F}^B$ arises from the thermal fluctuations in the fluid and is characterized by

$$\langle\mathbf{F}^B\rangle = 0 \quad \text{and} \quad \langle\mathbf{F}^B(0)\mathbf{F}^B(t)\rangle = 2kT\mathbf{R}_{FU}\delta(t) . \tag{3}$$

In Eq. (3) the angle brackets denote an ensemble average, k is Boltzmann's constant, T is the absolute temperature, and $\delta(t)$ is the delta function. The amplitude of the correlation between the Brownian forces at time 0 and at time t results from the fluctuation–dissipation theorem for the N-body system. On the time scales of interest, which are discussed below and are much longer than molecular times, the fluctuating forces can be considered instantaneous.

The Langevin equation (1) with the hydrodynamic force given by Eq. (2) and the Brownian force by Eq. (3) is valid provided the configuration of the particles does not change significantly during the time scale of the Brownian motion $\tau = m/6\pi\eta a$, where m is the mass of a particle, and a its size, i.e., during the time required for the particle's momentum to relax after a Brownian impulse.[8,25–27] Expressed as a fraction of the particle size, the change in the relative separation of two particles due to the Brownian displacement in the time τ is

$$\frac{(mkT)^{1/2}}{6\pi\eta a^2},$$

where use has been made of the Stokes–Einstein relation for the diffusivity of a single isolated particle $D_0 = kT/6\pi\eta a$. For micron-size particles in water at normal temperature, the above displacement is less than 10^{-3}. If two particles are very close together and $a\xi$ is the minimum distance between their surfaces, it is more proper to compare the relative displacement of the two particles during the time τ with $a\xi$; but then the relative diffusivity differs from that assumed above by a factor of order ξ, and the above is again an estimate of the change in the configuration in the time τ. Thus, for most situations of interest the configuration can be assumed constant during the Brownian relaxation time τ.

We should note at this point that using Eq. (1) with Eqs. (2) and (3) will not give the long-time tails (long time on the scale of τ) observed in the velocity autocorrelation function for a single Brownian particle. To obtain such long-time tails, either the fluid's compressibility or inertia must explicitly be taken into account.[26,27] However, since we shall be interested in the behavior on time scales large compared with τ, a particle will have experienced many uncorrelated Brownian impacts from the solvent molecules, and its subsequent motion is described by Eqs. (1)–(3) with the *steady* values for the hydrodynamic resistance functions in Eq. (2). It is the steady hydrodynamic functions (or zero frequency limit) that characterize the diffusion process for times larger than τ.[4,27]

The evolution equation for the particles is obtained by following Ermak and McCammon[8] and integrating Eq. (1) over a time step Δt that is large compared with τ, but small compared with the time over which the configuration changes. A second integration in time produces the evolution equation for the particle positions (both translational *and* orientational) with error of $O(\Delta t^2)$:

$$\Delta\mathbf{x} = \{\mathbf{U}^\infty + \mathbf{R}_{FU}^{-1}\cdot[\mathbf{R}_{FE}:\mathbf{E}^\infty + \mathbf{F}^P]\}\Delta t + kT\nabla\cdot\mathbf{R}_{FU}^{-1}\Delta t + \mathbf{X}(\Delta t) . \tag{4}$$

$\Delta\mathbf{x}$ is the change in particle position during the time step Δt. $\mathbf{X}(\Delta t)$ is a random displacement due to Brownian motion that has zero mean and covariance given by the inverse of the resistance matrix:

$$\langle\mathbf{X}\rangle = 0 \quad \text{and} \quad \langle\mathbf{X}(\Delta t)\mathbf{X}(\Delta t)\rangle = 2kT\mathbf{R}_{FU}^{-1}\Delta t . \tag{5}$$

Equation (4) simply states that the motion of a particle is composed of three parts, each resulting from the basic forces in Eq. (1). There is a deterministic contribution due to the hydrodynamic shear forces, $[\mathbf{U}^\infty + \mathbf{R}_{FU}^{-1}\cdot\mathbf{R}_{FE}:\mathbf{E}^\infty]\Delta t$, one due to the interparticle or external forces, $[\mathbf{R}_{FU}^{-1}\cdot\mathbf{F}^P]\Delta t$, and two contributions from Brownian motion: (1) a displacement due to the configuration space divergence of the N-particle diffusivity $[kT\nabla\cdot\mathbf{R}_{FU}^{-1}]\Delta t$ and (2) a random step $\mathbf{X}(\Delta t)$ whose properties are such that the fluctuation–dissipation theorem is satisfied.

Nondimensionalizing $\mathbf{x}$ by the particle size a; the time by the diffusive time scale a^2/D_0; the shear forces by $6\pi\eta a^2\dot\gamma$, where $\dot\gamma = |\mathbf{E}^\infty|$ is the magnitude of the shear rate; and the interparticle forces by their magnitude $|\mathbf{F}^P|$, the evolution equations (4) and (5) become

$$\Delta x = \mathrm{Pe}\{\mathbf{U}^{\infty} + \mathbf{R}_{FU}^{-1}\cdot[\mathbf{R}_{FE}:\mathbf{E}^{\infty} + \dot{\gamma}^{*-1}\mathbf{F}^{P}]\}\Delta t + \nabla\cdot\mathbf{R}_{FU}^{-1}\Delta t + \mathbf{X}(\Delta t)\,,$$
$$\langle\mathbf{X}\rangle = 0 \quad \text{and} \quad \langle\mathbf{X}(\Delta t)\mathbf{X}(\Delta t)\rangle = 2\mathbf{R}_{FU}^{-1}\Delta t\,. \tag{6}$$

Here, $\mathrm{Pe} = \dot{\gamma}a^2/D_0 = 6\pi\eta a^3\dot{\gamma}/kT$ is the Péclet number, which measures the relative importance of the shear and Brownian forces, and $\dot{\gamma}^* = 6\pi\eta a^2\dot{\gamma}/|\mathbf{F}^P|$ is a nondimensional shear rate giving the relative importance of shear and interparticle forces.

Equation (6) shows clearly that the behavior of the suspension depends on the dimensionless parameters: Pe, $\dot{\gamma}^*$, and ϕ, the volume fraction of particles. No restriction has been made to particles of identical size or shape; they need not be spherical, and if not other dimensionless parameters characterizing their shape would be present. If more than one type of particle is present, there would then be a volume fraction ϕ_i for each type. In general, there will also be other nondimensional parameters that characterize the range, rather than the amplitude, of the interparticle forces. Other situations, such as sedimentation, e.g., result in a similar nondimensionalization with a sedimentation rate setting the velocity scale rather than a shear rate. When the deterministic component of the particle motion is dominated by the imposed shear flow, the condition that the particle Reynolds number be small can be written as $\mathrm{Re} = \rho a^2\dot{\gamma}/\eta \ll 1$.

If Brownian motion is unimportant, i.e., $\mathrm{Pe}\to\infty$, it is appropriate to scale time with the shear rate $\dot{\gamma}$ rather than with the diffusive time a^2/D_0. This has the effect of dividing the right-hand side of Eq. (6) by Pe, so that Pe^{-1} now multiplies the Brownian contributions. Our previous dynamic simulation studies of suspensions[1,2] correspond to this limit. The "Brownian dynamics" simulations that have appeared in the literature[8–15] are all based on the limit $\mathrm{Pe}\to 0$ and are incapable of examining either the high Pe limit or concentrated suspensions because of the incomplete treatment of the hydrodynamic forces (see below). As developed here, Stokesian dynamics is completely general, encompassing both high and low Pe number limits as special cases.

Readers more comfortable with a continuum description of the suspension physics should know that Eq. (6) can also be obtained from a configuration space Fokker–Planck or Smolochowski equation for the N-particle probability distribution function $P(\mathbf{x})$, which is the appropriate level of description for times long compared with τ.[8] The conserved probability satisfies

$$\frac{\partial P}{\partial t} + \nabla\cdot\mathbf{v}P = 0\,. \tag{7}$$

The N-particle velocity results from the imposed flow and the forces acting on the particles and is given by

$$\mathbf{v} = \mathbf{U}^{\infty} + \mathbf{R}_{FU}^{-1}\cdot[\mathbf{R}_{FE}:\mathbf{E}^{\infty} + \mathbf{F}^{P} - kT\nabla\ln P]\,. \tag{8}$$

The terms in the bracket represent the velocity due to the shear, the interparticle and the Brownian forces, respectively. At the Fokker–Planck level, the fluctuating Brownian forces appear as a *thermodynamic* force $-kT\nabla\ln P$. Time integration of Eq. (7) with Eq. (8) over a short time step Δt results precisely in Eq. (6), showing the equivalence of the two descriptions.

The evolution equation (6) is the heart of the dynamic simulation. Given an initial configuration $\mathbf{x}(0)$, Eq. (6) is simply integrated in time to follow the dynamic evolution of the suspension *microstructure*. To use Stokesian dynamics to determine *macroscopic* properties of the suspension we must derive corresponding average expressions. These, in general, depend on the property to be investigated, and since our interest here is in diffusion we shall only discuss the appropriate averages for diffusion. (An application to rheology, where the macroscopic stress is determined, in the absence of Brownian motion has already appeared,[2] and a study of the rheology of Brownian suspensions is in progress.) The N-particle diffusion tensor $\mathbf{D}$ is related to the resistance and mobility matrices by the following:

$$\mathbf{D} \equiv kT\mathbf{R}_{FU}^{-1} = kT\mathbf{M}\,. \tag{9}$$

Several "particle diffusivities" may be defined, and here we shall be interested in the short- and long-time self-diffusivities. The short-time self-diffusivity $\mathbf{D}_0^s$ is given by an instantaneous average over all configurations and over all identical particles:

$$\mathbf{D}_0^s = \frac{1}{N}\langle\mathrm{tr}\,\mathbf{D}\rangle\,, \tag{10}$$

where tr stands for the sum (trace) of the diagonal elements of $\mathbf{D}$ corresponding to the N different particles. The angle brackets denote the average over all configurations sampled by the particles. The long-time self-diffusivity $\mathbf{D}_\infty^s$ is defined as the limit as time approaches infinity of one-half of the time rate of change of the mean-square position of a particle and is given by

$$\mathbf{D}_\infty^s = \lim_{t\to\infty}\frac{1}{2N}\frac{d}{dt}\langle\mathrm{tr}(\mathbf{x} - \langle\mathbf{x}\rangle)^2\rangle\,. \tag{11}$$

$\mathbf{D}_\infty^s$ measures the ability of a particle to wander far from its starting point, while $\mathbf{D}_0^s$ measures the instantaneous mobility of a particle in its local environment. Both are accessible by light scattering in tracer diffusion experiments, being the long- and short-wavelength scattering limits, respectively.[4,22] Intermediate time definitions are not possible as the motion of a particle is not, in general, diffusive except at short and long times. The collective-diffusion coefficient $\mathbf{D}^c$, measuring particle flux in response to a concentration gradient, is closely related to sedimentation and is not discussed here.[4,21,25,28–31]

B. Hydrodynamic Interactions

The evolution equation (6) and the definitions of the diffusivities (10) and (11) are exact for N particles. These expressions show clearly the fundamental importance of the hydrodynamic interactions embodied in the resistance matrix $\mathbf{R}_{FU}$, or its invert the mobility matrix $\mathbf{M}$. The entire evolution of the suspension microstructure *and* the macroscopically observed properties depend on these interactions, so an accurate representation of the N-body resistance matrices is essential. As mentioned in the introduction, both many-body interactions and lubrication need to be addressed. Previous Brownian dynamics simulations did not consider either of these effects. We have recently developed a general method to calculate the resistance matrices $\mathbf{R}_{FU}$ and

$\mathbf{R}_{FE}$ that accounts for the near-field lubrication effects and the dominant many-body interactions.[32] Here, we shall briefly summarize the method.

The resistance matrices $\mathbf{R}_{FU}$ and $\mathbf{R}_{FE}$ can be written as part of a "grand resistance" matrix $\mathscr{R}$, which relates the force/torque (F) and stresslet (S) exerted by the fluid on the particles to the particle velocities and the rate of strain:

$$\begin{pmatrix}\mathbf{F}\\ \mathbf{S}\end{pmatrix} = -\mathscr{R}\cdot\begin{pmatrix}\mathbf{U}-\mathbf{U}^{\infty}\\ -\mathbf{E}^{\infty}\end{pmatrix}, \tag{12}$$

$$\mathscr{R} = \begin{pmatrix}\mathbf{R}_{FU} & \mathbf{R}_{FE}\\ \mathbf{R}_{SU} & \mathbf{R}_{SE}\end{pmatrix}. \tag{13}$$

The corresponding inverse or "grand mobility" $\mathscr{M}$ representation is

$$\begin{pmatrix}\mathbf{U}-\mathbf{U}^{\infty}\\ -\mathbf{E}^{\infty}\end{pmatrix} = -\begin{pmatrix}\mathbf{M}_{UF} & \mathbf{M}_{US}\\ \mathbf{M}_{EF} & \mathbf{M}_{ES}\end{pmatrix}\cdot\begin{pmatrix}\mathbf{F}\\ \mathbf{S}\end{pmatrix}. \tag{14}$$

For just two spherical particles the grand resistance and mobility matrices are known exactly for all center–center separations. For N particles, short of solving the full N-body problem, some approximations are necessary. The method we have developed exploits the fact that the lubrication effects are most conveniently treated in the resistance formulation, while many-body interactions are more easily incorporated in the mobility formulation.

Starting from the integral solution for Stokes flow, in conjunction with Faxén laws for particle velocities, we form the N-sphere grand mobility matrix by expanding the force density on the surface of each particle in a series of moments. The zeroth moment is just the total force F, while the first moment has both antisymmetric and symmetric parts, being the torque L and stresslet S, respectively. Thus, each particle is replaced by its first few multipoles. In this moment's expansion, the mobility matrix $\mathbf{M}_{UF}$ coupling translation velocities and forces is the well-known Rotne–Prager tensor. The other matrices are of similar structure. The first neglected term in this moment's expansion comes from the quadrupole densities of the particles, and, since they are induced, the leading error in $\mathbf{M}_{UF}$ is $O(1/r^6)$, where r is a characteristic interparticle spacing. [The errors to the other mobility matrices in Eq. (14) are of even higher order.] Both $\mathscr{R}$ and $\mathscr{M}$ are symmetric and positive definite.

Once constructed, the grand mobility matrix, denoted $\mathscr{M}^{\infty}$, is inverted to yield a far-field approximation to the grand resistance matrix of Eq. (13). While the mobility matrix is pairwise additive, inverting it solves the many-body problem at the level of forces and stresslets; thus, the resistance matrix is a true many-body interaction. This is most easily seen by noting that $\mathbf{R}_{FU} \neq \mathbf{M}_{UF}^{-1}$. Rather, $\mathbf{R}_{FU} = (\mathbf{M}_{UF} - \mathbf{M}_{US}:\mathbf{M}_{ES}^{-1}:\mathbf{M}_{EF})^{-1}$; the second term is a stresslet rate of strain or "dipole–dipole" scattering term, propagating interactions through the effective medium. (The effective viscosity of a suspension of force/torque-free particles can be shown to be proportional to an average of $\mathbf{M}_{ES}^{-1}$.[19,33]) Note, however, that $\mathbf{R}_{FU}$ does equal $\mathbf{M}^{-1}$, the complete mobility matrix relating velocities and forces. We have shown that the inversion of the mobility matrix reproduces both the screening characteristic of a porous medium, which is the nature of a two-particle interaction in $\mathbf{R}_{FU}$ since all other particles are presumed fixed, and the effective viscosity of free suspensions.[32]

This many-body approximation to the resistance matrix still lacks, however, lubrication. Lubrication would only be reproduced upon inversion of the mobility matrix if all multipole moments were included. To include lubrication, we introduce it in a pairwise additive fashion in the resistance matrix. To each element of $(\mathscr{M}^{\infty})^{-1}$ we add the known exact two-sphere resistance interactions,[24,34,35] which we shall designate as $\mathscr{R}_{2B}$, for two-body resistance matrix. However, part of the two-sphere resistance interactions, the far-field part, has already been included upon the inversion of $\mathscr{M}^{\infty}$. Thus, in order not to count these interactions twice, we must subtract off the two-body interactions already included in $(\mathscr{M}^{\infty})^{-1}$, which are found by inverting a two-sphere mobility matrix to the same level of approximation as in $\mathscr{M}^{\infty}$. Denoting this resistance matrix as $\mathscr{R}_{2B}^{\infty}$, our approximation to the grand resistance matrix that includes near-field lubrication and far-field many-body interactions is

$$\mathscr{R} = (\mathscr{M}^{\infty})^{-1} + \mathscr{R}_{2B} - \mathscr{R}_{2B}^{\infty}. \tag{15}$$

The grand resistance matrix is then partitioned as in Eq. (13) and used in the evolution equation (6) and the calculation of the diffusivities (9)–(11). This procedure outlined above has been shown to give excellent results for both finite numbers of interacting particles and unbounded suspensions.[32,36]

The effort expended in constructing an approximation to the resistance matrix $\mathscr{R}$ is indicative of the complexity of the hydrodynamic interactions. The computational time grows as the number of degrees of freedom cubed (a matrix inversion and solution), and there are 11 degrees of freedom per particle in 3 dimensions (3 force, 3 torque, and 5 components of the symmetric and traceless stresslet), which is costly, but the intensive calculations are needed for three reasons.

First, lubrication forces are maintained only via the resistance formulation. Their importance can be appreciated by the following simple example. Given a chain of closely spaced particles, with a force applied to one particle at the end of the chain, the entire chain will move as if it were a rigid rod. The particles themselves never need come into contact, nor do they need to exert any interparticle nonhydrodynamic forces on one another. Lubrication alone suffices to move the entire chain. Such an effect cannot be captured by a pairwise additive approximation in a mobility formulation.

Second, we shall see in the next section that the procedure we have outlined above with purely hydrodynamic interactions produces the proper $g(r)$ for a hard-sphere system; no hard-sphere interparticle potential need be introduced. This is a nontrivial result and requires an accurate calculation of $\nabla\cdot\mathbf{R}_{FU}^{-1}$ in Eq. (6) when two or more particles are near contact. For near particles, $\nabla\cdot\mathbf{R}_{FU}^{-1}$ results in a relative radial velocity (of magnitude 1.6) that separates close pairs. This is essential, for the random displacement term in Eq. (6) has an amplitude that approaches zero linearly as particles come into contact, and particles placed in contact initially would remain in contact at all subsequent

times if this term were not present. It is the balance of $\nabla\cdot\mathbf{R}_{FU}^{-1}$ and the random displacement $\mathbf{X}$ in Eq. (6) that gives the proper hard-sphere distribution of particles. To accurately calculate the divergence of $\mathbf{R}_{FU}^{-1}$ we make use of the identity

$$\nabla\cdot\mathbf{R}_{FU}^{-1} = -\mathbf{R}_{FU}^{-1}\cdot\nabla\mathbf{R}_{FU}:\mathbf{R}_{FU}^{-1},$$

and analytically differentiate $\mathbf{R}_{FU}$.[37] Note, using only the Oseen or Rotne–Prager tensors this term is zero. Proper hard-sphere distributions cannot be obtained with these approximations without introducing a repulsive interparticle force.

Third, although it would appear that a simple pairwise additivity of velocities in the mobility formulation, i.e., using the Oseen or Rotne–Prager tensors for the hydrodynamic interactions between two particles, is an N^2 calculation as opposed to our N^3 formulation, to evaluate the random displacements in Eq. (6) essentially requires finding the eigenvalues of the mobility matrix $\mathbf{M}$, which is an N^3 operation. To see this, note that the random displacements $\mathbf{X}$ are to be chosen with zero mean and covariance $\langle\mathbf{XX}\rangle = 2\mathbf{R}_{FU}^{-1}\Delta t$. To accomplish this, $\mathbf{R}_{FU}$ is factored into an upper triangular matrix $\mathbf{A}$, $\mathbf{R}_{FU} = \mathbf{A}^T\cdot\mathbf{A}$, and inverted, $\mathbf{R}_{FU}^{-1} = \mathbf{A}^{-1}\cdot(\mathbf{A}^{-1})^T$. The random displacements $\mathbf{X}$ are then given by

$$\mathbf{X} = \sqrt{\Delta t}\,\mathbf{A}^{-1}\cdot\mathbf{Y},$$

where $\mathbf{Y}$ is a normal random variable of zero mean and covariance $\langle\mathbf{YY}\rangle = 2\mathbf{I}$. The factorization step, which is required regardless of whether $\mathbf{R}_{FU}$ or $\mathbf{M}$ is used, is itself an N^3 operation. Thus, once *any* hydrodynamic interactions between particles are included, an N^3 operation must be performed, and with little additional computational cost the *full* hydrodynamic interactions can be used.

Finally, one may note that inverting the grand mobility matrix need not be performed at each time step. Variations in $\mathscr{M}^\infty$ occur when particles have moved a distance of order their size a. Because of the lubrication singularities (which are of the form $1/\xi$) variations in $\mathbf{R}_{FU}$ occur when particles move a distance of order their separation $a\xi$ and so a multiple time-stepping procedure can be used. In general, $\mathscr{M}^\infty$ is inverted only once every 20 or so time steps.

The final element necessary to simulate unbounded suspensions is the use of periodic boundary conditions. We use the same procedure as outlined in our previous simultation studies of sheared suspensions.[1,2] Some difficulties have arisen with the use of periodic boundary conditions when simulating three-dimensional suspensions of hydrodynamically interacting particles; specifically, the mobility matrix has lost positive definiteness, resulting in negative eigenvalues and imaginary random displacements.[9] This aphysical result comes about from not properly accounting for the long-range interactions in suspensions and is completely avoided by following the method we have developed in Ref. 36. This method forms rigorously convergent particle interactions by correctly accounting for the "back flow" of fluid[28,38] In the monolayer simulations to be discussed in the next section, where all particles lie in the same plane, many of the convergence difficulties present in three-dimensional suspensions are absent, and it is not necessary to explicitly take the back-flow effects into account. That is, the mobility and/or resistance matrix formed as outlined above with periodic boundary conditions never lost positive definiteness, and simulations of a monolayer with the back-flow effects gave statistically the same results. Furthermore, we shall see in the next section that the above procedure produces the correct $g(r)$ in a dense suspension, which can only be obtained through a proper treatment of both the near- and the far-field hydrodynamic interactions. For a further elaboration on this point see Ref. 36.

III. RESULTS AND DISCUSSION

Our initial study has been the simulation of a sheared monolayer suspension of identical spheres that interact solely through hydrodynamic and Brownian forces. In a monolayer all particles lie in the same plane, the plane of the shear flow which is taken to be the (x,y) plane, and there are now only six degrees of freedom for each particle: F_x, F_y, L_z, and three components of the stresslet; S_{xy}, $S_{xx}-S_{zz}$, and $S_{yy}-S_{zz}$. In place of the volume fraction ϕ, we now have an areal fraction $\phi_A = N\pi a^2/A$, where N is the number of particles in a periodic cell of area A. The particle trajectories are calculated from Eq. (6) for a given shear rate $\dot\gamma = 2E_{xy}$ with no interparticle force $\mathbf{F}^P = 0$. The time step Δt is chosen as large as possible, but not so large that the configuration changes significantly. This requirement is actually very stringent owing to the Brownian motion. The relative displacement of two near particles due to the advective term in Eq. (6) $\Delta\mathbf{x}_a = \nabla\cdot\mathbf{R}_{FU}^{-1}\Delta t$, is $O(\Delta t)$ since $\nabla\cdot\mathbf{R}_{FU}^{-1}\sim O(1)$ as the surface separation ξ approaches zero. To insure that this displacement is small compared to ξ, the length over which $\mathbf{R}_{FU}$ changes, requires $\Delta x_a/\xi = \Delta t/\xi < 1$, or $\Delta t < \xi$. Similarly, the random relative displacement of near particles coming from $\mathbf{X}(\Delta t)$ is $\Delta x_r \sim \sqrt{|\mathbf{R}_{FU}^{-1}|\Delta t} \sim \sqrt{\xi\Delta t}$. For this to be small compared with ξ requires $\Delta x_r/\xi = \sqrt{\xi\Delta t}/\xi < 1$, or again $\Delta t < \xi$. In both cases we require Δt small compared with ξ. We have found that $\Delta t \sim 10^{-3}$ gives reasonable values for the number of near neighbors as $\xi\to 0$ (r near 2) and is not too prohibitive in terms of computation times. It should be noted, however, that some particle overlap will occur because the random displacement is $O(1)$ for $\xi\sim O(10^{-3})$. The statistical information to be presented was for runs of at least 10 000 time steps, after an equilibration period of 2500 time steps. All runs were performed with 25 particles, with the exception of some results for $\mathrm{Pe} = 0$ and ∞, where 49 particles were used. The areal fraction has been kept constant at $\phi_A = 0.453$ and the Péclet number varied from zero to infinity. Table I summarizes the relevant information and some results.

A. Pair-distribution function

Shown in Fig. 1 is a comparison of the radial distribution function obtained by Stokesian dynamics for the purely Brownian case $\mathrm{Pe} = 0$, with that for a system of hard disks at the same areal fraction obtained by a Monte Carlo calculation.[39] The agreement is seen to be excellent. The maximum error of $\approx 3\%$ occurs at contact ($r = 2$) and is the same size as the statistical uncertainty in the simulation results (two separate runs of 10 000 steps each gave less than approxi-

TABLE I. Presented are the results of the simulation of a monolayer of 25 identical hard spheres at an areal fraction $\phi_A = 0.453$ for several values of the Péclet number $\mathrm{Pe} = \dot{\gamma}a^2/D_0 = 6\pi\eta a^3\dot{\gamma}/kT$. The short- and long-time self-diffusion coefficients D_0^s and D_∞^s, respectively, are normalized by the diffusivity of a single isolated sphere $D_0 = kT/6\pi\eta a$. $g(2)$ is the angularly averaged value of the pair-distribution function at contact. The final two columns give the time step, nondimensionalized by $\dot{\gamma}^{-1}$ in all but the pure Brownian case $\mathrm{Pe} = 0$, where a^2/D_0 is used, and the number of steps over which statistical averages were computed after an equilibration period of 2500 steps.

Pe	D_0^s	D_∞^s	$g(2)$	Δt	No. steps
0	0.74 ± 0.01	0.49 ± 0.02	2.62 ± 0.05	10^{-3}	30 000
1	0.74 ± 0.01	0.49 ± 0.04	2.9 ± 0.1	10^{-3}	10 000
10	0.69 ± 0.01	2.7 ± 0.2	8.0 ± 0.5	10^{-3}	20 000
100	0.66 ± 0.01	22 ± 1	57 ± 3	2×10^{-3}	10 000
1000	0.61 ± 0.01	74 ± 4	380 ± 30	2×10^{-3} and 10^{-2}	10 000
∞	0.57 ± 0.01	$\to\infty$	$\to\infty$	2×10^{-3}	40 000

mately 3% difference.) This good agreement indicates that the slight amount of particle overlapping caused by the time step limitation is not detrimental.

The statistics of a monolayer of identical spheres must be the same as that of a two-dimensional hard-disk fluid. That these two are the same is most easily seen from the Fokker–Planck analysis of Eqs. (7) and (8). At equilibrium the particle flux must vanish and Eq. (8) gives the Boltzmann distribution for particle centers

$$P_{\mathrm{eq}} \sim \exp[-V(\mathbf{x})/kT],$$

where we have $\mathbf{E}^\infty = 0$ and have written $\mathbf{F}^P = -\nabla V$, with V the N-particle hard-sphere (or hard-disk) potential. Although it is true that the Boltzmann distribution must be obtained regardless of what hydrodynamics are used, to obtain $g(r)$ through simulation, where there are no interactions other than hydrodynamic ($\mathbf{F}^P = 0$), is a nontrivial result. It may at first seem surprising that through simulation the correct $g(r)$ is obtained with the interparticle force set equal to zero, $\mathbf{F}^P = 0$, while the Fokker–Planck equation requires that we write $\mathbf{F}^P = -\nabla V(\mathbf{x})$, the gradient of the hard-sphere potential. There is no conflict here because the hard-sphere potential results in repulsive interparticle forces that are delta functions located on the particle surfaces $\delta(\xi)$, where ξ is the dimensionless surface–surface separation, i.e., the force is only nonzero when particles touch. In the evolution equation (6) these forces are multiplied by $\mathbf{R}_{FU}^{-1}$, and the relative mobility of two particles vanishes when they touch. Thus, the velocity a particle receives from the hard-sphere repulsion is proportional to $\xi\delta(\xi)$, which is zero; with hydrodynamic interactions, the hard-sphere potential has no dynamical significance. As mentioned in Sec. II, in simulation it is the proper balance between the deterministic advective step $\nabla\cdot\mathbf{R}_{FU}^{-1}\Delta t$ and the random displacement $\mathbf{X}(\Delta t)$ in Eq. (6) that results in the correct $g(r)$. Only through a proper treatment of the hydrodynamic interactions, both near- and far-field, will a correct $g(r)$ be obtained by simulation; these results show that our method is accurate.

In Fig. 2 we show $g(r)$ for three different Péclet numbers: $\mathrm{Pe} = 0$, 10, and ∞. The pair-distribution function is not independent of the angle θ in the plane of shear (cf. Fig. 3), and the reported $g(r)$ are angular averages of $g(r,\theta)$. $\mathrm{Pe}\to\infty$ corresponds to purely hydrodynamic interactions, i.e., no Brownian motion. The values of $g(r)$ at contact for all Pe simulated are given in Table I. The major feature to note is the increasing value of $g(r)$ at contact with increasing Pe, and the attendent sharpening of the second nearest-neighbor peak. The sharp peak at contact indicates the formation of aggregates or clusters of particles in very close

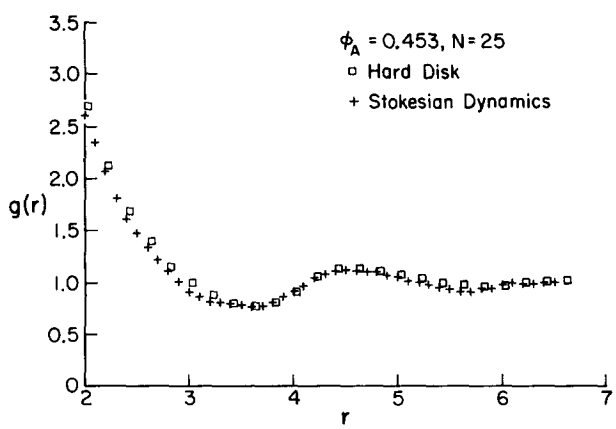

FIG. 1. The radial dependence of the pair-distribution function $g(r)$ determined by simulation (+) is compared to that of a hard-disk fluid (□) at the same areal fraction $\phi_A = 0.453$ determined by a Monte Carlo calculation in Ref. 39.

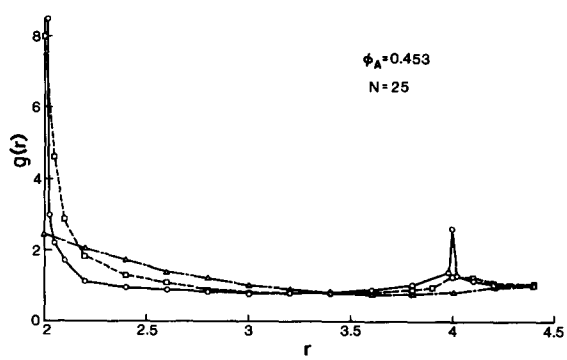

FIG. 2. A comparison of the pair-distribution function (angularly averaged) determined by simulation for three different values of the Péclet number: (△), $\mathrm{Pe} = 0$; (□), $\mathrm{Pe} = 10$; (○), $\mathrm{Pe}^{-1} = 0$.

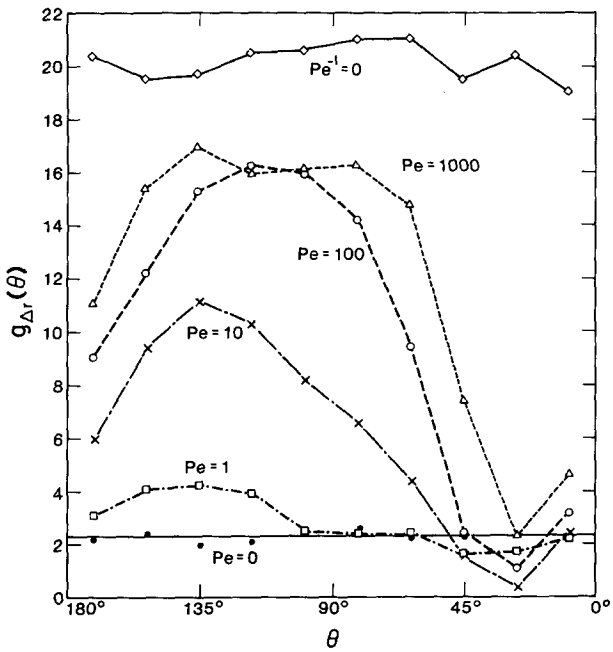

FIG. 3. The angular dependence of the pair-distribution function $g_{\Delta r}(\theta)$ in the radial range $2<r<2.05$ for six values of the Péclet number: -●- Pe = 0, -□- Pe = 1, -x- Pe = 10, -○- Pe = 100, -△- Pe = 1000, -◇- Pe^{-1} = 0. $90°<\theta<180°$ is upstream of the reference particle, and $0<\theta<90°$ downstream. $g_{\Delta r}(\theta)$ in the first and third quadrants and in the second and fourth quadrants are the same.

contact ($\xi < 10^{-3}$) as Pe increases. This cluster formation has a profound influence on suspension rheology[2] and will be seen below to significantly affect the long-time diffusive behavior.

In addition to the changing radial dependence, the pair-distribution function undergoes an even more pronounced angular development with changing Pe. This is illustrated in Fig. 3 where the angular dependence of the pair-distribution function near contact $g_{\Delta r}(\theta)$ for the radial range $2\leqslant r\leqslant 2.05$ is plotted as a function of θ for Pe = 0, 1, 10, 100, 1000, and ∞. $\theta = 180°$ is upstream of the reference particle, $\theta = 0°$ is downstream, and the angular dependencies in the first and third quadrants and in the second and fourth quadrants are the same. The purely Brownian limit (Pe = 0) has, of course, no angular structure. As the Péclet number increases, angular structure develops, with an increase in the number of near neighbors on the upstream side $90°<\theta<180°$ and a decrease on the downstream side $0°<\theta<90°$. In the purely hydrodynamic limit (Pe^{-1} = 0) there is a slight angular structure, but it is symmetric about $\theta = 90°$, a property not present at any other Péclet number other than zero. Indeed, perturbation analysis for small Pe shows that $g_{\Delta r}(\theta) \sim \sin 2\theta$ to first order in Pe.[40] We can see in Fig. 3 that a Pe = 1 already deviates from the linear regime.

The asymmetry in $g_{\Delta r}(\theta)$ about $\theta = 90°$ is reminiscent of that observed in our simulations of suspensions with repulsive interparticle forces[1,2] and a similar interpretation can be given. On the upstream side, the shear flow is advecting particles towards the central one and the buildup is balanced by a diffusive flux outward. On the downstream side, the shear flow carries particles away and the deficit of particles is balanced by a diffusive flux towards the central particle. Only in the linear regime of small Péclet number, and therefore small deformation, are the surplus and deficit of the same magnitude and a sin 2θ dependence of $g(r,\theta)$ obtained. The asymmetric $g(r,\theta)$ displayed in Fig. 3 is also indicative of the presence of normal stress differences in the rheology of these Brownian suspensions.[41]

B. Short-time self-diffusion

The short-time self-diffusion coefficients $\mathbf{D}_0^s$ are reported in column 2 of Table I. The reported values are x and y averages, i.e., $\mathbf{D}_0^s = \frac{1}{2}(D_{xx} + D_{yy})$. $\mathbf{D}_0^s$ is an instantaneous, configurational average and measures the average mobility of a particle in the local structure present at each value of Pe. The short-time self-diffusivity decreases as Pe increases owing to the formation of close pairs and larger aggregates (cf. Figs. 2 and 6). Because of lubrication forces, a pair of closely spaced particles moves for a short time as if it were a single larger particle and there is a corresponding decrease in mobility. Recall that the mobility, and therefore the self-diffusion coefficient, scales as one over the particle size. Although the change in $\mathbf{D}_0^s$ with Péclet number does not seem large, it should be realized that $\mathbf{D}_0^s$ in three-dimensional Brownian suspensions (Pe = 0) only varies from 0.47 to 0.25 as ϕ is increased from 0.3 to 0.45.[18] Thus, the change from 0.74 to 0.57 with increasing Péclet number at the *same* areal fraction represents a significant change due to the changing microstructure.

C. Long-time self-diffusion

The long-time self-diffusion coefficients $\mathbf{D}_\infty^s$, which are also reported in Table I, follow from the definition (11) and are determined by calculating the average trajectories $\langle x^2(t)\rangle$, $\langle x(t)y(t)\rangle$, and $\langle y^2(t)\rangle$ by simulation. Because of the simple shear flow, the displacements $\langle x^2\rangle$ and $\langle xy\rangle$ do not grow linearly with time, but have the following nondimensional long-time behavior:

$$\begin{aligned}
&\langle x^2(t)\rangle = 2D^s_\infty t\left[1 + \tfrac{1}{3}(\mathrm{Pe}\, t)^2\right],\\
&\langle x(t)y(t)\rangle = D^s_\infty\, \mathrm{Pe}\, t^2,\\
&\langle y^2(t)\rangle = 2D^s_\infty t. \qquad (16)
\end{aligned}$$

Here $D^s_\infty = D_{yy}$, only the yy component of the diffusion tensor can be determined. Equation (16) is simply the solution for the mean-square displacement of a passive diffusing scalar released at the origin in an unbounded simple shear flow and should describe the long-time behavior of a Brownian particle.[42] In the simulations, the sudden jumps in position associated with the periodic boundary conditions are removed, so that the trajectories followed are those that would occur in an unbounded fluid.

We first note from Table I that the long-time self-diffusivity at Pe = 0 is smaller than the short-time self-diffusivity. This is as expected, for the diffusing particle must deform the local structure, breaking out of its "cage" of near neighbors and changing places with its neighbors. Such behavior has recently been observed experimentally by van Megen, Underwood and Snook[22] in concentrated hard-sphere colloidal

dispersions. While a quantitative comparison is not possible between our monolayer simulations and the three-dimensional experiments, the decreases in the two situations are of similar magnitude. This decrease in the long-time self-diffusivity associated with a cage effect is illustrated in Fig. 4, where $\langle y^2 \rangle$ is plotted vs t. Once a particle has diffused a distance of order its size ($\sqrt{\langle y^2 \rangle} \approx 1.6$), it must deform the local structure and is slowed down significantly. One can see the slowing down associated with the first and second nearest-neighbor shells. Figure 4 also shows that the behavior at $\mathrm{Pe} = 1$ is qualitatively and quantitatively similar to that at $\mathrm{Pe} = 0$.

At higher Péclet number, however, the behavior of the long-time self-diffusivity is quite different. Table I shows the values of $\mathbf{D}^s_\infty$ *on the scale of* D_0. On purely dimensional arguments, as $\mathrm{Pe} \to \infty$ one expects the dimensional $\mathbf{D}^s_\infty$ to scale as $\dot{\gamma} a^2$, or dimensionless terms $\mathbf{D}^s_\infty \sim \mathrm{Pe}$ as $\mathrm{Pe} \to \infty$. This behavior is verified by the data in Table I. Because of the different scales in the Brownian ($\mathrm{Pe} \to 0$) and hydrodynamic ($\mathrm{Pe} \to \infty$) regimes, it is difficult to compare the behaviors for Péclet numbers greater than or less than unity. In Fig. 4 we see the curve for $\langle y^2 \rangle$ at $\mathrm{Pe} = 10$ rising rapidly because the time is being measured in diffusion times a^2/D_0 rather than in shear rate units $\dot{\gamma}^{-1}$. The best simulataneous comparison of the different behaviors is shown in Fig. 5, where $\langle y^2 \rangle / t$ is plotted vs t for the six values of the Péclet number. For $\mathrm{Pe} = 0$ and 1, time is measured in units of a^2/D_0, while for $\mathrm{Pe} = 10$, 100, 1000, and ∞ time is measured in units of $\dot{\gamma}^{-1}$. The high Péclet number curves show that the short time behavior is deterministic, with $\langle y^2 \rangle \sim t^2$, and only after several characteristic times does the diffusive behavior set in. Measured in terms of the mean displacement of a particle, the diffusive behavior sets in after a particle has moved of order it size, i.e., $\sqrt{\langle y^2 \rangle} \approx 1$. Similarly, at low Péclet number the long-time behavior sets in after a particle has moved a distance of order its size, but the behavior is neither deterministic nor diffusive during this relaxation time, which is seen from Fig. 5 to be of order four diffusion times.

For $\mathrm{Pe}^{-1} = 0$, $\langle y^2 \rangle / t$ has not reached an asymptote by a time of 12. It is clear that the motion is not deterministic — $\langle y^2 \rangle$ is not proportional to t^2, but it does not appear diffusive. The explanation for this unusual behavior is the formation of very large clusters, encompassing most of the particles, which slowly rotate with the average angular velocity of the bulk flow and deform due to the extensional components of the motion. This is illustrated in Fig. 6 where "snap shots" of particle configurations at two arbitrary instants in time are shown for 49 particles at (a) $\mathrm{Pe} = 0$ and (b) $\mathrm{Pe}^{-1} = 0$. Note the absence of large clusters and a well dispersed arrangement of particles in the Brownian limit. This is to be contrasted with the cell spanning cluster encompassing most of the particles that is oriented along the compressive axis of the shear flow in the pure hydrodynamic case. The lines in the particle indicate the translational motion of the particles relative to the average shear flow, and show that clusters display complex internal dynamics, as particles move within a cluster, but do not necessarily leave it. There thus appears to be a slowly evolving, quasiperiodic motion that strongly influences the displacement of a particle. This is evident in the velocity autocorrelation function where oscillations about zero are seen for $t > 2$. The introduction of a small amount of Brownian motion $\mathrm{Pe}^{-1} = 0.001$ reduces these os-

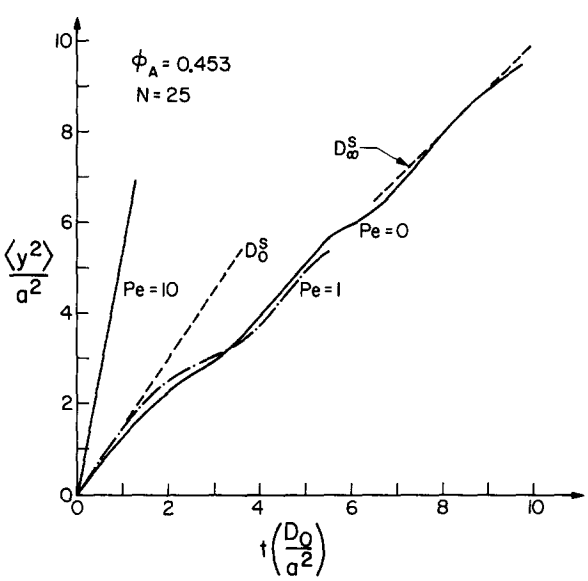

FIG. 4. The mean-square displacement $\langle y^2 \rangle$ vs t for $\mathrm{Pe} = 0$, 1, and 10. Note the changes in slope for $\langle y^2 \rangle \approx 2.5$ and 6 demarking the passage of the first and second nearest-neighbor shells. The dashed straight lines show the limiting diffusion coefficients.

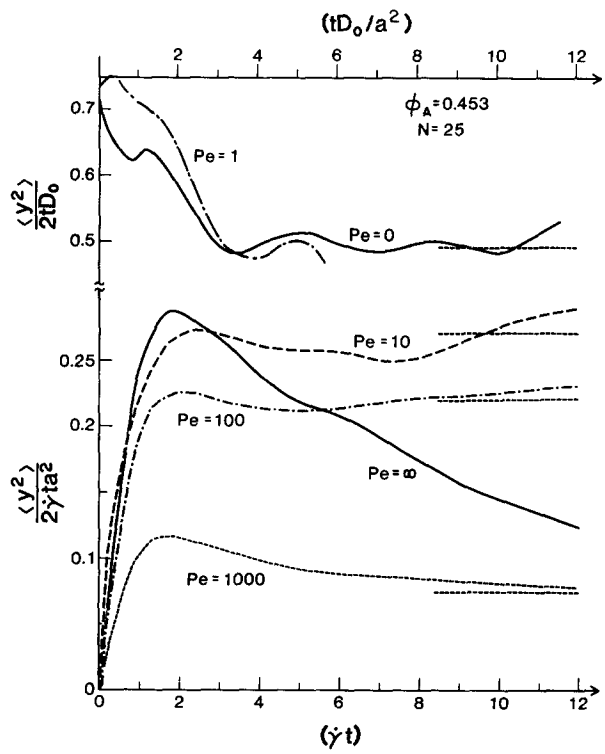

FIG. 5. The mean-square y displacement divided by time: $\langle y^2 \rangle / 2t$ for all values of the Péclet number. For $\mathrm{Pe} = 0$ and 1, the time is measured in units of the diffusion time scale a^2/D_0, for $\mathrm{Pe} = 10$, 100, 1000, and ∞, the time is measured in shear rate units $\dot{\gamma}^{-1}$. The dashed horizontal lines show the limiting long-time self-diffusion coefficients. Note the characteristic relaxation times for obtaining the long-time limit.

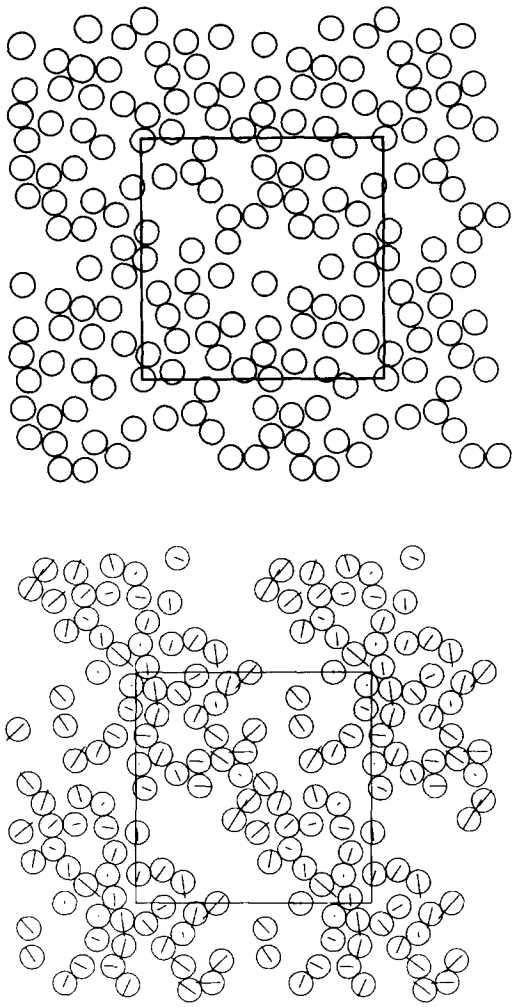

FIG. 6. Snap shots of particle configurations for 49 particles in the (a) pure Brownian limit ($Pe = 0$) and (b) the pure hydrodynamic limit ($Pe^{-1} = 0$). Note the absence of large clusters and the well dispersed arrangement of particles in the Brownian limit, and the very large spanning cluster along the compressive axis (135°) of the shear flow in the hydrodynamic limit. The lines in the particles in (b) give the particle translational motion relative to the average shear flow. The slow evolution of the large clusters results in a very long relaxation time for attaining the diffusive limit for $Pe^{-1} = 0$ as seen in Fig. 7.

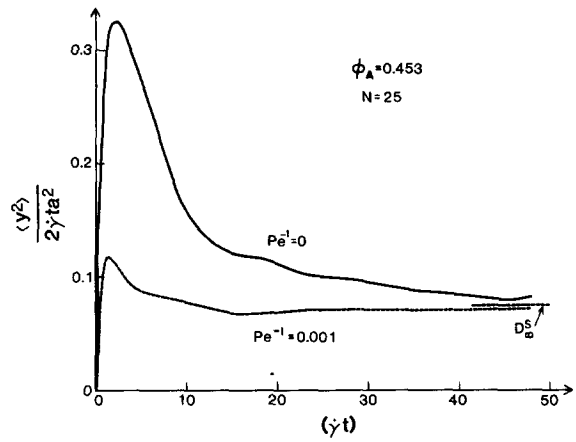

FIG. 7. The mean-square displacement divided by time $\langle y^2 \rangle / 2t$ for $Pe^{-1} = 0$ and 0.001. After a very long time the pure hydrodynamic case has achieved an asymptotic diffusive behavior. The horizontal dashed line is the long-time self-diffusivity.

cillations and a well-behaved diffusive regime sets it. At the same time, all other statistical measures such as D_0^s, the effective viscosity, etc., have stabilized and do not display any of this transitory behavior.

The evolution of the clusters results in very slow dynamics as far as particle displacements are concerned. This is shown in Fig. 7, where $\langle y^2 \rangle / t$ for $Pe^{-1} = 0$ and 0.001 is plotted vs t over a much longer time scale. After very long times the pure hydrodynamic limit seems to have reached an asymptote giving roughly the same lone-time diffusivity as at $Pe^{-1} = 0.001$. It should be noted that it is not the "randomness" introduced by Brownian motion for Pe^{-1} nonzero that results in the rapid obtainment of a diffusive behavior; rather, it is the fact that a small amount of Brownian motion, primarily through the action of $\nabla \cdot \mathbf{R}_{FU}^{-1}$, breaks clusters and surpresses their rotary motion. This has been verified through simulation by studying the behavior at $Pe = 10^4$ with and without the $\nabla \cdot \mathbf{R}_{FU}^{-1}$ term. In the absence of this term the behavior is qualitatively the same as at $Pe^{-1} = 0$, while with this term the behavior is quite similar to that at $Pe = 10^3$.

There have been recent experiments by Leighton and Acrivos[43] on suspensions of purely hydrodynamically interacting particles that have measured this "shear induced" self-diffusion coefficient for $Pe^{-1} = 0$, showing that it does indeed scale as $\dot{\gamma}a^2$. In the purely hydrodynamic regime, the evolution equations for the particle positions form a set of conservative, autonomous nonlinear ordinary differential equations of dimension $2N$, and one expects to observe chaotic trajectories and diffusive behavior for such systems, just as one observes diffusive behavior for hard spheres in vacuum. Our simulation runs seem to confirm this, although the slow evolution of the cluster dynamics makes it difficult to obtain runs of long duration. The run up to a time of 48 is only just comparable with the shortest times over which Leighton and Acrivos experimentally measured the shear-induced self-diffusion coefficient. It should also be appreciated that any effect, such as very short-range repulsive forces, that acts to destroy clusters may significantly affect the time scale for obtaining the long-time diffusive regime and the value of the diffusivity. We note in passing that plots of $\langle xy \rangle / t^2$ and $\langle x^2 \rangle / t^3$ gave statistically the same diffusivities as $\langle y^2 \rangle / t$, indicating the correctness of Eq. (16).

Finally, in Fig. 8 we show a log–log plot of $\mathbf{D}^s_\infty$ vs Pe. This curve shows clearly a Brownian motion dominated regime for $Pe < 1$, where $\mathbf{D}^s_\infty \sim O(1)$, and a hydrodynamically dominated regime for $Pe > 10$, where $\mathbf{D}^s_\infty \sim O(Pe)$. The rather dramatic change in $\mathbf{D}^s_\infty$ from $Pe = 10^2$ to $Pe = 10^3$, and subsequently for larger Pe, is a direct result of the lubrication forces. The small amount of Brownian motion at $Pe^{-1} = 0.001$ has destroyed the largest clusters, but particle pairs still come into very close contact, which slows down their relative motion. [Order of magnitude considerations show that a significant population of particle pairs will be at a separation ξ of $O(Pe^{-1})$ where advection and diffusion balance.] By extrapolating the asymptotic behaviors to their

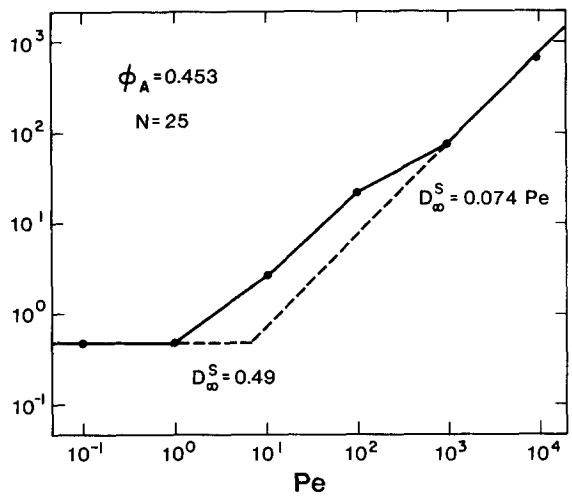

FIG. 8. The long-time self-diffusivity normalized by the infinite dilution diffusivity D_0 is plotted as a function of the Péclet number. The dashed lines are the limiting asymptotes: $D^s_\infty \sim 0.49$ as $\mathrm{Pe} \to 0$ and $D^s_\infty \sim 0.074$ Pe as $\mathrm{Pe} \to \infty$. The transition from the Brownian motion dominated regime to the hydrodynamically dominated regime occurs for $\mathrm{Pe} \approx 10$. Note, as $\mathrm{Pe} \to \infty$, the dimensional long-time self-diffusivity scales as $\dot{\gamma}a^2$.

point of intersection we obtain a Péclet number of approximately 10, for the transition from one regime to the other. Such a form is expected for other suspension properties, such as the effective viscosity, and can be quite useful in identifying the regions of Brownian and hydrodynamic dominance.

IV. CONCLUSIONS

We have presented in this paper a general and flexible method for dynamically simulating the behavior of concentrated suspensions of Brownian particles. The Stokesian dynamics method is capable of predicting both microstructural and macroscopic properties of colloidal dispersions. The microstructural properties illustrated here were the pair distribution functions; the macroscopic properties were the self-diffusivities. The method we have developed captures the essential physics of the hydrodynamic interactions in a suspension; specifically, both the dominant many-body interactions and the near-field lubrication forces are explicitly included. The simulation method passes continuously and smoothly from pure Brownian motion ($\mathrm{Pe} = 0$) to pure hydrodynamics ($\mathrm{Pe}^{-1} = 0$), no change in approach or procedure is needed.

In our study of self-diffusion in simple shear flow of a monolayer of identical spheres we have seen the clear demarkation between a diffusion or Brownian motion dominated regime, $\mathrm{Pe} \to 0$, and a hydrodynamically dominated regime, $\mathrm{Pe} \to \infty$, with a crossover around $\mathrm{Pe} \approx 10$. This is most evident in Fig. 8 where the long-time self-diffusivity D^s_∞ changes from being independent of the Péclet number at small Péclet number, to growing linearly with it at high Péclet number. The transition can also be detected in the pair-distribution functions shown in Figs. 2 and 3. The pronounced sharpening of the first nearest-neighbor peak for $\mathrm{Pe} > 10$ is characteristic of the formation of closely spaced aggregates or clusters, a result of the lubrication forces.

This aggregate formation plays a very important and central role in the behavior of suspensions. We saw that in the purely hydrodynamic regime $\mathrm{Pe}^{-1} = 0$, the formation of large clusters, and their subsequent tumbling and stretching motions, dominated the long-time displacement of a tracer particle, making it difficult to extract a hydrodynamic diffusion coefficient in this limit. The presence of a small amount of Brownian motion, $\mathrm{Pe}^{-1} = 0.001$, destroyed the large clusters and a well-behaved diffusive behavior set in. It should be emphasized that it is only the large clusters that are destroyed, the small clusters, i.e., pairs of particles, are not significantly affected by a small amount of Brownian motion. This is seen by noting that the first nearest-neighbor peak, at least on the upstream side of the central particle, is of the same magnitude as that in the purely hydrodynamic limit. Visual evidence is also present in Fig. 6.

Other evidence for this breaking of large clusters while preserving small ones is the behavior of the short-time self-diffusion coefficient. One can attempt a simple interpretation of the decrease in D^s_0 with increasing volume fraction ϕ as due to a single particle diffusing in a viscous medium with the effective viscosity at that value of ϕ. All our simulations were carried out at the same value of the areal fraction, and the only change in effective viscosity that can occur is that due to the changing microstructure. (Note, there is an additional "direct" contribution to the bulk stress from the Brownian motion itself,[40] which is not considered here and is not important for these arguments.) We showed in a previous study[2] that a pairwise additive calculation of the viscosity is relatively insensitive to changes in the pair-distribution function. Thus, the slowing down of the short-time self-diffusion coefficient with increasing Péclet number cannot be viewed uniquely as a particle moving in an increasingly viscous fluid. Rather, clusters of increasing size form as the Péclet number increases, and a particle cannot move, even at short times, without moving all members of the compact cluster.

A similar effect was observed in our simulations of hydrodynamic particles with short-range repulsive forces.[2] Even a small amplitude repulsive force [$\dot{\gamma}^* \gg 1$ in the notation of Eq. (6)] was effective at breaking the very large clusters, but the small clusters, as measured by the pair-distribution function, were not significantly perturbed. In this case, the suspension viscosity was dramatically reduced by the destruction of the large clusters. All of these results indicate the tremendous importance the microstructure, specifically the cluster formation, has on determining suspension properties. The connectivity aspects brought about by the lubrication forces are paramount in understanding and predicting suspension behavior.

Here we have studied one of the simplest Brownian suspensions—hard spheres with only Brownian and hydrodynamic forces. It should be clear from our derivation of the evolution equation in Sec. II that many other, more complex suspension problems can be addressed. The rheology of such pure hydrodynamic and Brownian suspensions is straightforward to determine and is in progress. Interparticle forces, such as London–van der Waals and electrostatic, or external forces such as gravity, are easy to incorporate. The complex-

ity of the problem increases of course, where now, in addition to ϕ and Pe, parameters characterizing the interparticle forces must be varied. Another interesting application of Stokesian dynamics is to study the behavior of micromechanical models of polymers. One need no longer treat either freely draining Rouse models or preaveraged hydrodynamics as in the Zimm model[44,45]; the complete hydrodynamic problem can now be addressed.

ACKNOWLEDGMENTS

This work was supported in part by NSF Grant Nos. CBT-8451597 and INT-8413695 and by the Centre de Calcul Vectoriel pour la Recherche.

[1]G. Bossis and J. F. Brady, J. Chem. Phys. **80**, 5141 (1984).
[2]J. F. Brady and G. Bossis, J. Fluid Mech. **155**, 105 (1985).
[3]B. J. Berne and R. Pecora, *Dynamic Light Scattering* (Wiley, New York, 1976).
[4]J. M. Rallison and E. J. Hinch, J. Fluid Mech. **167**, 131 (1986).
[5]D. J. Evans and H. J. M. Hanley, Phys. Rev. A **20**, 1648 (1979).
[6]D. J. Evans, H. J. M. Hanley, and S. Hess, Phys. Today **37** (1), 26 (1984).
[7]D. J. Evans and W. G. Hoover, Annu. Rev. Fluid Mech. **18**, 243 (1986).
[8]D. L. Ermak and J. A. McCammon, J. Chem. Phys. **69**, 1352 (1978).
[9]E. Dickinson, Chem. Soc. Rev. **14**, 421 (1985).
[10]J. Bacon, E. Dickinson, and R. Parker, Faraday Discuss. Chem. Soc. **76**, 165 (1983).
[11]E. Dickinson, S. A. Allison, and J. A. McCammon, J. Chem. Soc. Faraday Trans. 2 **81**, 591 (1985).
[12]G. C. Ansell, E. Dickinson, and M. Ludvigsen, J. Chem. Soc. Faraday Trans. 2 **81**, 1269 (1985).
[13]G. C. Ansell and E. Dickinson, J. Colloid Interface Sci. **110**, 73 (1986).
[14]G. C. Ansell and E. Dickinson, J. Chem. Phys. **85**, 4079 (1986).
[15]K. Gaylor, I. Snook, and W. van Megen, J. Chem. Phys. **75**, 1682 (1981).
[16]C. W. J. Beenakker and P. Mazur, Phys. Lett. A **91**, 290 (1982).
[17]C. W. J. Beenakker and P. Mazur, Physica A **120**, 338 (1983).
[18]C. W. J. Beenakker and P. Mazur, Physics A **126**, 349 (1984).
[19]C. W. J. Beenakker, Physica A **128**, 48 (1984).
[20]W. van Megen, I. Snook, and P. N. Pusey, J. Chem. Phys. **78**, 931 (1983).
[21]A. B. Glendinning and W. B. Russel, J. Colloid Interface Sci. **89**, 124 (1982).
[22]W. van Megen, S. M. Underwood, and I. Snook, J. Chem. Phys. **85**, 4065 (1986).
[23]H. Brenner and M. E. O'Neill, Chem. Eng. Sci. **27**, 1421 (1972).
[24]S. Kim and R. T. Mifflin, Phys. Fluids **28**, 2033 (1985).
[25]G. K. Batchelor, J. Fluid Mech. **74**, 1 (1976).
[26]E. J. Hinch, J. Fluid Mech. **72**, 499 (1975).
[27]W. B. Russel, Annu. Rev. Fluid Mech. **13**, 425 (1981).
[28]G. K. Batchelor, J. Fluid Mech. **52**, 245 (1972).
[29]G. K. Batchelor, J. Fluid Mech. **119**, 379 (1982).
[30]G. K. Batchelor and C.-S. Wen, J. Fluid Mech. **124**, 495 (1982).
[31]G. K. Batchelor, J. Fluid Mech. **131**, 155 (1983).
[32]L. Durlofsky, J. F. Brady, and G. Bossis, J. Fluid Mech. **180**, 21 (1987).
[33]G. K. Batchelor, J. Fluid Mech. **41**, 545 (1970).
[34]D. J. Jeffrey and Y. Onishi, J. Fluid Mech. **139**, 261 (1984).
[35]P. A. Arp and S. G. Mason, J. Colloid Interface Sci. **61**, 21 (1977).
[36]J. F. Brady, R. Phillips, J. Lester, and G. Bossis, J. Fluid Mech. (submitted).
[37]Since the mobility invert part of $\mathbf{R}_{FU}$ from Eq. (15) is not known analytically, this expression is "run backwards" and $\mathbf{M}_{UF}$ analytically differentiated for this term.
[38]R. W. O'Brien, J. Fluid Mech. **91**, 17 (1979).
[39]D. G. Chae, F. H. Ree, and T. Ree, J. Chem. Phys. **50**, 1581 (1969).
[40]G. K. Batchelor, J. Fluid Mech. **83**, 97 (1977).
[41]Note, to leading order in Pe the normal stress differences are zero. They first appear at $O(\mathrm{Pe}^2)$.
[42]A. S. Monin and A. M. Yaglom, *Statistical Fluid Mechanics* (M.I.T., Cambridge, 1965), Vol. I.
[43]D. T. Leighton and A. Acrivos, J. Fluid Mech. **177**, 109 (1987).
[44]R. Byron Bird, O. Hassager, R. C. Armstrong, and C. F. Curtiss, *Dynamics of Polymeric Liquids. Vol. II. Kinetic Theory* (Wiley, New York, 1977).
[45]H. H. Saab and P. J. Dotson, J. Chem. Phys. **86**, 3039 (1987).